Journal of Materials Science: Materials in Electronics (2020) 31:12502–12513
https://doi.org/10.1007/s10854-020-03798-6

Cooperative effects due to Ca substitution by La on the normal and superconducting states of (Bi, Pb):2223 system

A. Sedky[1] · Amna Salah[1] · A. A. Bahgat[2] · Aly Abou-Aly[3]

Received: 23 April 2020 / Accepted: 12 June 2020 / Published online: 9 July 2020

Abstract
The normal and superconducting properties of $Bi_{1.7}Pb_{0.30}Sr_2Ca_{2-x}La_xCu_2O_y$ (Bi, Pb):2223 system with various x values ($0.00 \le x \le 0.30$) have been reported. It is found that the replacement of Ca^{2+} by La^{3+} up to 0.30 does not influence the phase purity of the pure system, while the orthorhombic distortion, excess oxygen, effective Cu valance and hole carriers/Cu ions are clearly affected. Further, the doping distance and crystal geometry factor are decreased, but the distance between neighboring Cu-atoms and density of excess doping are increased. Furthermore, the DTA diagrams show strong endothermic peaks T_m at 844.1, 848, 850.1 and 857.4 °C for pure and La samples, respectively. The mass loss determined by TGA displayed a sharp mass loss started at about 800 °C and extended to 1000 °C for all samples. Although the critical temperatures T_c of the samples are decreased by La insertion from 119 to 104, 71, and 53 K, the critical concentration for quenching superconductivity may be extended above 0.30. On the other hand, the Vickers hardness H_v is increased by La up to 0.30, but it is decreased by the applied load F. Additionally, a negative linear relation between T_m or H_V and T_c is obtained as due to cooperative interactions, ($T_c \propto -T_m$) i.e. there are an extended forces acting along such a wide temperature range. The H_v–F characters are divided into two linear parts; the first at lower loads (0.00–1.96 N) and the second at higher loads (2.94–4.90 N). The variation of surface energy Υ against La is different according to the range of applied loads, while the elastic indentation d_e is decreased, and the resistance pressure F_o is increased. But, the values of F_o and d_e at higher loads are generally more than that of lower loads, while the vice is versa for the Υ. Our results are discussed in terms of the balance between the hole carriers lost by La^{3+} with that introduced by excess oxygen in the Cu–O_2 planes.

1 Introduction

It is known that superconductivity, SC, phenomenon is cooperative in nature. Normally, cooperative phenomenon is that when there are several entities that are taking part to produce the physical phenomena in question. According to Matthias [1] superconductivity is one of the cooperative phenomenon that may correlate normal to the superconducting states properties. That is to say, the macroscopic properties such as melting temperature and mechanical properties are correlated to the critical SC temperature.

In the present study, we will consider Bi(Pb):2223 superconducting system with a critical temperature T_C of 110 K, where it has three CuO_2 planes and the superconductivity occurs at these planes, while the other layers such as Sr–O, CaO and Bi–O are non-superconductors [2, 3]. Due to large number of CuO_2 planes and also the difficulty to mix of Bi(Pb):2212 minority phase with Bi:2223 majority phase, it is not easy to obtain a single-phase free from intergrowths in such a system, and consequently T_C vary between 106 and 110 K [4, 5]. However, heat treatment during Bi(Pb):2223 synthesis may supports increasing the content of the Bi-2223 phase relative to the amount of the Bi-2212 phase [6, 7]. On the other hand, the partial substitution of Bi by Pb has been used to stabilize and improve the formation of its original phase, as well as the superconducting critical parameters [8]. For example, the highest values of the critical temperature, T_c, critical fields, H_c, and critical current, I_c, are obtained when Pb = 0.30 [9].

Generally, the unit cell of Bi (Pb):2223 compound with $a \sim b = 0.544$ nm and $c = 3.600$ nm consists of

✉ A. Sedky
sedky196000@hotmail.com; sedky1960@yahoo.com

[1] Physics Department, Faculty of Science, Assiut University, Assiut, Egypt

[2] Physics Department, Faculty of Science, Al-Azhar University, Cairo, Egypt

[3] Physics Department, Faculty of Science, Alexandria University, Alexandria, Egypt

$Bi_{1.7}Pb_{0.30}Sr_2Ca_2Cu_3O_{10+\delta}$ unit and about 19 layers and planes. It is approved that the chemical formula of 10-oxygen atoms (10 O^{2-}) needs at least 20 electrons provided by $1.7Bi^{3+} + 0.30Pb^{2+} + 2Sr^{2+} + 2Ca^{2+} + 3Cu^{2+}$ ions. To be superconductor, this compound should be over doped with excess oxygen atoms by transforming $3Cu^{2+}$ ions into $3Cu^{3+}$ ions, and therefore, the electronic arrangement becomes $1.7\ Bi^{3+} + 0.30Pb^{2+} + 2Sr^{2+} + 2Ca^{2+} + 3Cu^{3+} + 11O^{2-}$ [2].

The melt process is considered as the highly essential method for optimization of thermal behavior of superconductors through solid–liquid phase diagram. Furthermore, the transition points such as melting, sublimation and solidification can be obtained. Differential thermal analysis (DTA) and thermo-gravimetric analysis (TGA) are considered for identifying the above points [10]. TGA is a powerful technique to explore the thermal stability of a material through accurately monitoring the weight of a sample and heating at a constant rate. The change in the sample weight during thermal treatments is attributed to a specific material response due to thermal stress. This is the perfect way for exploring, in detail, decomposition temperatures and ensuring a material performs adequately in a given temperature range. DTA is used for measuring the temperature difference between the sample and the standard reference for obtaining solid–liquid phase diagram. However, DTA up to 1000 °C with 10 °C/min heating rate was considered earlier to investigate the amount of Bi (Pb):2223 phase relative to the amounts of other phases such as Bi (Pb):2212 phase. The DTA show that the structure of Bi (Pb):2223 phase is more stable and can be easily prepared as stable pure phase rather than Bi (Pb):2212 phase [11].

Generally, chemical substitution plays a crucial role in high T_c superconductors, and consequently the substitution into (Bi, Pb):2223 system have been carried out to improve their normal and superconducting properties [12–25]. However, it is approved that the superconducting properties depend on the density of holes carriers in the CuO_2 planes as well as the effective Cu-valance [26–28]. Therefore, the substitution of Ca^{2+} ions by RE^{3+} elements (rare earth in the lanthanum series) leads to a decrease of the formal Cu-valence state, and ultimately T_c decreases [29, 30]. The excess of positive charge for trivalent RE^{3+} cation, as compared to divalent Ca^{2+} cation, causes repletion between CuO_2 planes, thereby the separation between these planes may be increased. Furthermore, the increase of RE content induces excess oxygen incorporated between the Bi_2O_3 double layers [31]. In this respect, (Bi, Pb):2223 system holds some advantage in that the oxygen stoichiometry is relatively invariant with respect to RE^{3+} substitution when the samples are prepared in an identical environment [32–34].

Most of the studies have concluded that even though RE^{3+} improves the stability of Bi: 2223 structure, the critical parameters show a degrading tendency as the doping concentration increases [19, 35–39]. On the other hand, very few studies show an improvement of T_c in Bi(Pb):2223 systems [40–44]. Regardless of the RE^{3+} elements which already show superconductivity in the RE: 123 phases such as Y, Gd, Sm and Nd in lanthanide series while only few studies were based on La. Additionally, the ionic size of La^{3+} (1.18 Å) is higher than that of Ca^{2+} (1.12 Å), if the substitution occurs at the same eightfold coordination sites. Although, the substitution of La at Ca position in BSCCO systems show a decrease of the superconducting properties, a question mark should be considered as due to T_c variations by such substitution. Anyhow, the answer is still unclear and needs to pay more attentions, especially for higher La^{3+} content that is up to 0.30 as due to the non-superconducting phases of $Bi_2Sr_2CaLaCu_3O_y$ compound [45].

On the other hand, high T_c superconductors, HTS, have relatively poor mechanical properties, which may limit their practical applications. In this aspect, Vickers microhardness testing is considered as a convenient method for investigating the mechanical properties of bulk specimens. Where the elastic deformation is observed when the deformation is due to very small-applied loads. While above a critical loads a plastic (irreversible) deformation is produced. Generally, indentation size effect (ISE) occurs when the microhardness decreases as the applied load increases [46, 47]. While, the reverse indentation size effect occurs when the microhardness increases with the applied load [45–47]. However, the improved mechanical properties of Bi:2223 system may be achieved by substitution of RE^{3+} ions at Ca^{2+} site [48, 49]. It is found that RE^{3+} substitution improve the connection between grains, and consequently the mechanical resistance is increased [10, 50–52].

As an extension to the above works, a systematic study on the normal and superconducting properties of $Bi_{1.7}Pb_{0.30}Sr_2Ca_{2-x}La_xCu_2O_y$ (Bi, Pb):2223) with various, x, values ($0.00 \le x \le 0.30$) is reported. On the light of the present work we are able to increase the T_c of pure sample to 119 K. Further, it is shown that although the superconducting critical temperatures are decreased by La^{3+} substitution, the critical concentration for quenching superconductivity is increased to about 0.50. Furthermore, the relation between the normal state properties, such as melting temperature, T_m, hardness, H_V, Young's modulus, E, and yield strength, Y, and the superconducting critical temperature state property, T_c, are studied and correlated to shade some light on their association. Moreover, the distance between neighboring Cu-atoms, density of excess doping, decomposition temperature, hole carries/Cu ions. However, these findings are discussed in terms of the resulting hole carriers due La^{3+} and excess oxygen.

2 Experimental

The required amounts of Bi_2O_3, SrO, La_2O_3, $CaCO_3$ and CuO oxides and carbonates of 4 N purity $Bi_{1.7}Pb_{0.30}Sr_2Ca_{2-x}La_xCu_2O_y$ (Bi, Pb):2223) are thoroughly mixed and calcinated at 825 °C in air for 24 h. The calcination process is repeated three times with intermediate grinding at each stage. The resulting powder regrounded, and pressed into pellets at a force up to 10 tons, then sintered in air at 850 °C for 150 h and cooled down to room temperature at the rate of (5°/min). For optimizing the excess oxygen in the samples, the pellets are finally annealed in air at 850 °C for 20 h and left in the furnace for slow cooling to room temperature. The phase purity of the samples is examined by using X-ray diffraction pattern (PhilipsPW-1700) with Cu–Kα radiation of ave length λ = 1.5418 Å at 40 kV and 30 mA settings, and the data diffraction angle range (20°–70°) with a step of 0.06 in order to evaluate crystalline phase and crystallite orientation. The DTA and TGA thermal analysis are performed from room temperature up to 1000 °C with heating rate of 10 °C/min. The melting behaviors of the samples are analyzed by Schimadzu differential thermal analyzer-50 (DTA). The electrical resistivity of the samples is obtained by using the standard four-probe technique in closed cycle cryogenic refrigerator within the range of (18–300) K (Displex) employing helium gas. A 1.0 mA dc current, *I*, is supplied by a digital Keithley 6221 constant current source and the dc voltage drop, *V*, in the normal and reverse directions across the sample is measured by dc Keithley 181 digital nanovoltmeter. High-quality silver paint is used for electrical ohmic contacts. A calibrated chromel versus gold with 0.07 at.% iron (Kp-Au 0.07 at.% Fe) thermocouple is used for recording the sample temperature. The electrical resistivity of the sample is obtained using the relation,, where *w*, *L* and *t* are the sample width, length and thickness, respectively. Finally, the Vickers microhardness of the samples at room temperature are determined using manual microhardness tester model IN-412A with an applied loads of (0.49–10 N).

3 Results and discussion

3.1 Structural analysis

The theoretical and measured densities ρ_{th} and ρ_{exp} of the samples are listed in Table 1. ρ_{th} is calculated from XRD analysis using the relation, $\rho_{th} = \frac{M}{2N_A a^3}$, where N_A is the Avogadro's number, M is the molecular weight of the sample and a is the unit cell lattice parameter. While, ρ_{exp} is obtained for the samples using Archimedes principle in terms of the buoyant force F_B and volume using the relation, $\rho_{exp} = \frac{F_B}{gV}$. It is clear that both values increased by increasing La content, however the values of ρ_{th} are higher than that of ρ_{exp}. The porosity of the samples, $PS = [1—(\rho_{exp}/\rho_{th})]$, listed in Table 1 is decreased by La content due to decreasing the vacancies [53, 54].

It is evident from XRD pattern shown in Fig. 1 that all samples are single phase and are free from any impurity phases. The peaks of high intensity indicated by *H* (*hkl*) belong to the Bi(Pb):2223 phase, while the peaks of very low intensity indicated by *L* (*hkl*) intensities such as (131), (115), (019) (240), (172), (310) and (3110) belong to Bi(Pb):2212 phase. However, the composition of low 2212

Table 1 Lattice parameters, *c*/*a*, OD, *D*, *β*, V_{2212}%, *ρ* and *PS* for the samples

La content	*a* (Å)	*b* (Å)	*c* (Å)	*c*/*a*
0.00	5.374 ± 0.003	5.390 ± 0.004	36.872 ± 0.043	6.862
0.05	5.373 ± 0.005	5.393 ± 0.005	36.816 ± 0.021	6.852
0.15	5.370 ± 0.004	5.401 ± 0.003	36.778 ± 0.022	6.849
0.30	5.355 ± 0.010	5.398 ± 0.010	36.768 ± 0.046	6.867
La content	OD	V_{2223} (%)	*D* (nm)	β $(nm)^{-2}$
0.00	0.003	78.58	16	0.004
0.05	0.004	70.08	19	0.003
0.15	0.006	74.75	22	0.002
0.30	0.008	80.73	27	0.001
La cont	ρ_{exp} (g/cm^3)	ρ_{th} (g/cm^3)		PS
0.00	5.72	6.40		0.106
0.05	5.92	6.44		0.081
0.15	6.29	6.65		0.054
0.30	6.51	6.68		0.025

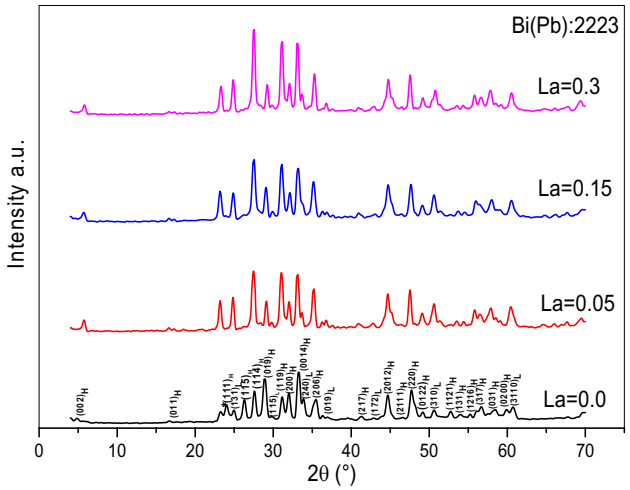

Fig. 1 XRD patterns for the samples

superconducting phase ($T_c = 89$ K) is normally formed as a minority phases in 2223 high phase, and cannot be consider as an impurity phase [22, 23, 51]. Furthermore, these peaks have very lower intensities as indicated above.

The volume fractions of the 2223 phase (V_{2223}) in the samples are determined by using the relation [55, 56]:

$$V_{2223} = \frac{\sum I_{2223}(\text{peaks})}{\sum I_{2223}(\text{peaks}) + \sum I_{2221}(\text{peaks}) + \sum I_{\text{other}}(\text{peaks})} \quad (1)$$

where I_{2223} is the peak intensity of 2223 phase, I_{2212} is the peak intensity of 2212 phase and I_{other} is the peak intensity of any other phases. As listed in Table 1, the V_{2223} fraction of the samples are 78.58%, 70.08%, 74.75% and 80.73%, respectively.

The average crystallite size D_{hkl} is evaluated in terms of Scherer's equation [57–59]:

$$D_{hkl} = \frac{k\lambda}{\Delta\theta \cos\theta} \quad (2)$$

where $\lambda_{\text{XRD}} = 15.418$ nm, $\Delta\theta$ is the half maximum line width, θ is the Bragg angle and $k = 0.9$. By using the Lorentz square method, the D_{hkl} values are listed in Table 1. On the other hand, the dislocation density is given as, $\beta = 1/D^2$ and are listed in Table 1 as well, indicating that the samples have very few lattice defects and are of good crystalline quality [60].

The lattice parameters a, b and c are listed in Table 1. The lattice parameters a and c are gradually decreased by increasing La content, while "b" increases. Similar behavior has been reported previously during substitution of rare-earth elements at Ca sites in Bi (Pb):2223 system such as Y, Er, Dy and/or Nd [20–23]. However, the decrease in the "c" parameter may be related to the amount of excess oxygen arising from the replacement of 2CaO by La_2O_3. The BiO double layers take up this excess oxygen and causing a tighter binding in these layers [38, 42, 61]. Consequently, the length of the in-plane Cu–O bond is decreased and helpful for reducing the "a" parameter. Otherwise, the increase in the "b" parameter is related to the change of hole carrier concentration per Cu ion within these planes [53–56]. This together with the ratio (c/a) is generally used to characterize the Jahn–Teller distortion of the oxygen octahedron around Cu^{2+} [62, 63]. Alternatively, the orthorhombic distortion, $OD = (b - a)/a$, given in Table 1 is increased by increasing La content, although c/a is decreased. The change of the unit cell parameters indicates that La release the John–Teller distortion of the CuO_6 octahedron markedly [64].

Furthermore, the oxygen content, y, is obtained by titration using the following formula [64]:

$$H = \left[\left(\frac{V_1 m_2}{V_2 m_1}\right) - 1\right]; \quad y = 10 + 1.5H \quad (3)$$

where V_1, V_2 are the volumes of $Na_2S_2O_3$ solution and m_1, m_2 are the masses of the sample during the first and second titration. The oxygen content listed in Table 2, indicating that La assist more excess oxygen to the system (y is higher than 10 for all samples). On the other hand, the effective Cu^{eff} valance can also be obtained with the help of the valence state of the compound elements (Bi^{+3}, Pb^{+2}, Sr^{+2}, Ca^{+2}, La^{+3} and O^{-2}) using the relation:

$$Cu^{\text{eff}} = \frac{2y - [9.7 + 2(1 - x) + 3x]}{3} \quad (4)$$

where x is the La content. Increasing La content as well as y increases the values of Cu^{eff}, as listed in Table 2.

The formation of 2223 high T_c phase generally requires the existence of Cu^{3+} ions in the superconducting planes as well as excess oxygen in/or near to CuO_2 planes [65–68].

Table 2 The y, Cu^{eff}, Σ, d, z and CGF for the samples

La cont	y	Cu^{eff}	$\Sigma^{1/2}$	Σ^{-1}	d (Å)	z (Å)	CGF
0.00	10.074	2.816	11.668	0.007	62.70	12.02	56.8×10^{-70}
0.05	10.124	2.833	9.036	0.012	48.55	12.01	29.7×10^{-70}
0.15	10.365	2.960	5.329	0.035	28.62	12.01	7.1×10^{-70}
0.30	10.526	3.017	4.473	0.050	23.96	11.97	3.7×10^{-70}

It is supposed that the Coulomb potential caused by excess oxygen atoms pins and distributes the doped holes in the CuO_2 planes to minimize their total energy as possible [3]. The density of excess doping, $\sum^{-1}$, due to excess oxygen is given by; $\sum^{-1} = (1 - 10y^{-1})$ [69, 70]. The excess oxygen can be also converted into a doping distance, d, given by; $d = a\sqrt{\sum}$, where $\sum$ is the hole doping density. Furthermore, the distance, z, between two neighboring Cu-atoms can be calculated by:

$$z = \sqrt{\left[(2a)^2 + a^2\right]} = a\sqrt{5}$$

Moreover, the crystal geometry factor (*CGF*) of the area of superconducting planes can be obtained by [3, 69, 70]:

$$CGF(\mathrm{Jm^2Kg}) = \left[(2d)^2 n^{-3/2} 2\pi K_B T_c m_{\mathrm{eff}}\right] = 6.31 \times 10^{-54} d^2 T_c n^{-3/2} \quad (5)$$

where n is the number of CuO_2 planes ($n = 3$ for the 2223 phase) and m_{eff} is the effective mass of the hole doped cup rates ($m_{\mathrm{eff}} = 2m_e = 18.210^{-31}$ kg). We basically used the above mathematical calculations to check the response of La cations in pure 2223 system. The calculated values of d, $\sum^{-1}$, z and *CGF* for La free and La containing samples are listed in Table 2. It is clear that both d, z and *CGF* are gradually decreased by increasing La content, while $\sum^{-1}$ is increased. Decreasing the doping distance d and also increasing the density of excess hole doping $\sum^{-1}$ by La are considered as the clear evidence for the increase of the hole carriers concentration, and consequently the distance between Cu-atoms z is decreased as obtained.

3.2 DTA, TGA analysis

Figure 2a shows the DTA patterns of the samples. It is noted that by increasing the temperature above RT, some exothermic and endothermic peaks with lower intensity are observed. These peaks are shifted to higher temperature as La content increases. They are shifted from the temperature range of (30–200 °C) to (200–450 °C), (450–700 °C) and (650–800 °C) for La pure and substituted samples. This is corresponding to crystallizations of 2201, 2212 and $(Sr,Ca)_2CuO_3$ phases, and also transformation of 2212 to 2223 phases. While with increasing temperature to about 800 °C, the tendencies of 2212 crystallization is completely disappear. Interestingly, the strong endothermic peaks listed in Table 3 occurred at 848.55, 855.24, 857.93 and 874.05 °C as La content increases, while no other strong peaks could be recorded, which reinforces the purity of the samples. This may be due to the decomposition reaction of 2223 superconducting phase. The increase of melting temperature by La may be attributed to increasing the optimum temperature of

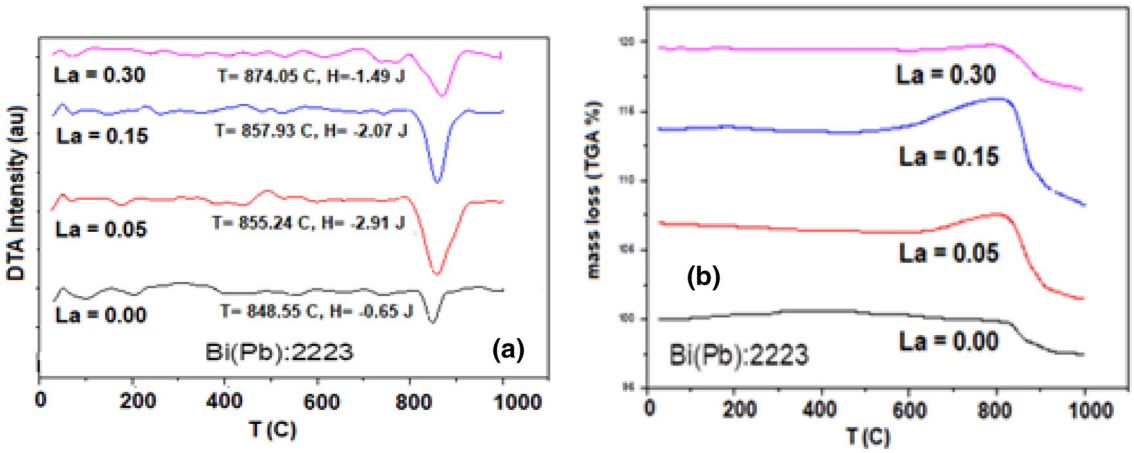

Fig. 2 **a** DTA and **b** TGA diagrams for the samples

Table 3 T_m, heat at the peak, ΔT (°C) and mass loss % for the samples

La content	T_m (°K) (DTA)	DTA peak heat (J)	ΔT (°C) TGA	TGA mass loss %	ΔT (°C) TGA	TGA mass loss %
0.00	1121.55	− 0.65	(39–741)	0.016	(747–989)	− 2.51
0.05	1128.24	− 2.91	(31–624)	− 0.670	(630–995)	− 4.88
0.15	1130.93	− 2.07	(34–568)	0.083	(574–986)	− 5.48
0.30	1147.05	− 1.49	(37–624)	− 0.148	(627–991)	− 2.80

the mixture due to La, which facilitates the growth of the 2223 phase. Such observed increase in T_m emphasizes the role of La addition on the internal structure of the examined samples. This behavior will be correlated in terms of the SC, T_c, values in the following section. On the other hand, the activation energy related to the endothermic heat are listed in Table 3, which is increased from 0.651 J for La-free sample to 2.91, 2.07 and 1.49 J as La content increases, in agreement with previously reported results [71, 72]. These results indicated that La addition increases the melting temperature of 2223 phase without producing any other additional compound as indicated from the above XRD results.

The TGA graph on the other hand shown in Fig. 2b indicates that the La containing samples with La = 0.00, 0.05 and 0.30, respectively, displaying a gradual mass loss starting from 40 °C to about 600 °C, followed by a significant mass gain at about 800 °C, followed by a sharp mass loss at about 1000 °C. However, the sample with $x = 0.15$ shows a mass gain starting from 40 °C up to about 400 °C, followed by a mass loss up to about 1000 °C. Furthermore, the temperature region of mass gain above 600 °C is completely disappeared. It is obvious that a gradual mass loss is due to de-oxidization of the samples, where the mass gain is due oxidation. However, a sharp mass gain close to 800 °C may be due to the decomposition temperature as indicated by the DTA analysis. Nevertheless, the increase of mass loss/mass gain is due to more excess of oxygen introduced by La doping [10, 11, 73]. Additionally, the oxygen content of the samples is calculated in terms of TGA mass loss for YBCO123 (Y:123) using the relation [74];

$$y = \left(\alpha + \frac{x}{2}\right) + \frac{l}{m-l}\left(\frac{M}{16}\right) \tag{6}$$

where $\boldsymbol{\alpha}$ is a parameter ($\alpha = 3.5$) for Y:123 system, x is the doping content, m is the mass of the sample, l is the average mass loss and M is the atomic weight. Substituting by the values of l and m deduced from TGA and also y obtained from iodometric titration, we found that ($\alpha = 8.08$) for the 2223 phase.

3.3 Resistivity measurements

Figure 3 depicts the electrical resistivity versus temperature for the samples. From this Figure it can be observed that the resistivity decreases almost linearly from room temperature and beyond which it turns to the superconducting state at the critical temperature T_c. It is also noted that all samples exhibit a clear metallicity which starts to decrease slightly by La addition. The linear part of the $\rho(T)$ curves has a positive slope $d\rho/dT$ and its extrapolation to $T = 0$ K provides the residual resistivity ρ_o. Usually, ρ_o is connected to the impurity scattering and $d\rho/dT$ is connected with carrier–carrier scattering [21, 75]. However, the values of normal state

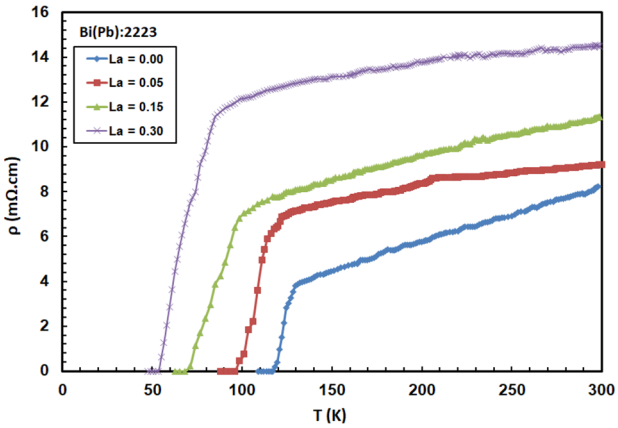

Fig. 3 Resistivity versus temperature for pure and La samples

resistivity ρ_{300} at 300 K, residual resistivity ρ_o at 0 K, T_c and width of transition ΔT_c for all samples are presented in Table 4. It is noted that the values of both ρ_o, ρ_{300} and ΔT_c are increased by La, while, T_c and $d\rho/dT$ is decreased. Interestingly, the T_c values are 119 K for pure sample and decreased to 104, 71 and 53 as La content increases. Therefore, we could improve the T_c of pure sample up to 119 K and also 104 K for La = 0.05. (The highest reported value is 110 K for the pure Bi-2223 sample [2–4]). This increase may be due to the final annealing period which is done during sample synthesis.

Next it is useful to consider the perspective reported in refs [39, 61] concerning the substitution of RE^{3+} in exchange of Ca^{2+} in Bi(Pb):2223 system. The reported data of reduced critical temperature $[T_c(x)/T_c(0)]$ against RE^{3+} content are drawn and shown in Fig. 4a. For comparison, our present results are included within the same Figure. It is clear that the critical concentration x_c of La for quenching superconductivity can be extended above 0.30, which is more than that reported earlier (0.35) for Gd, Sm and Nd elements [20, 22, 43, 45]. This behavior indicates that La has a higher solubility in Bi(Pb):2223 system and less detrimental to the superconductivity. However, different solubility's of rare-earth elements RE^{3+} in Bi(Pb):2223 system can be understood by a comparison of their ionic radii at eightfold coordination with respect to Ca^{2+} [76]. The reported data have indicated that the solubility of RE^{3+} in Bi(Pb):2223 system decreased as one move towards the rest of the lanthanide series, which are not given in the present case.

As reported above by Matthias [1] superconductivity is related to one of the cooperative phenomenon in nature and which may be correlated, to some normal state properties. This is examined here as shown in Fig. 4b which shows the relation between T_c as obtained from electrical conductivity measurements and T_m as obtained from DTA. As can be seen from the Figure, an inverse linear relation between T_m and

Table 4 The ρ_{300}, ρ_o, dρ/dT, T_c, T_{on}, $T_c(x)/T_c(0)$, ΔT_c, and p for the samples

La content	ρ_{300} (mΩ cm)	ρ_o (mΩ Cm)	dρ/dT (mΩ cm/K)	T_c (K)	T_{on} (K)	ΔT_c (K)	p
0.00	8.24	1	0.024	119	129	10	0.16
0.05	9.22	5.5	0.013	104	122	18	0.20
0.15	11.34	6	0.019	71	96	25	0.23
0.30	14.48	12	0.010	53	85	31	0.24

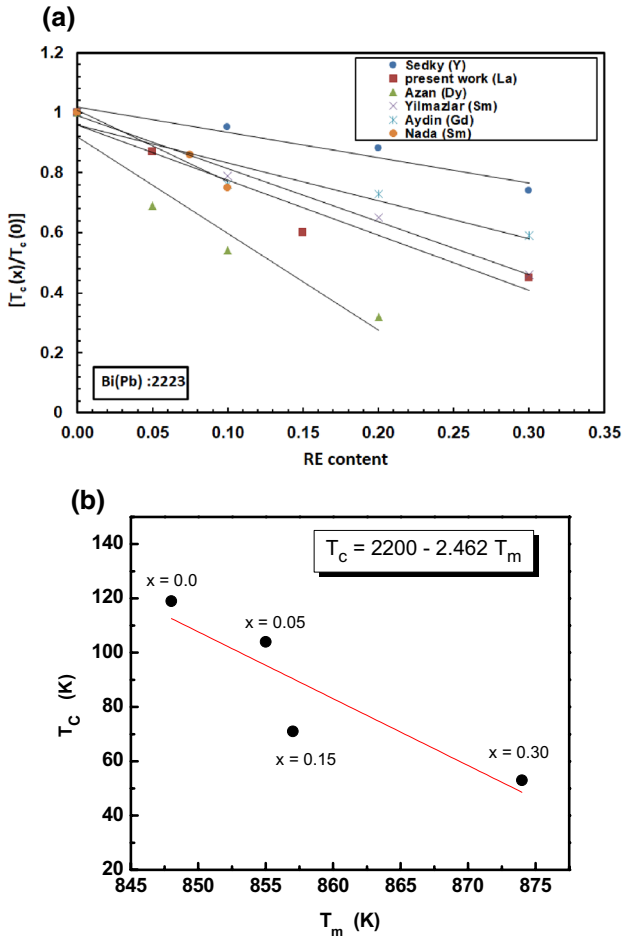

Fig. 4 **a** $[T_c(x)/T_c(0)]$ versus RE content for the present and reported data. **b** Relation between T_m and T_c for the samples

T_c is obtained and is given by; T_c (K) = 2200 − 2.462 T_m, as estimated. This behavior is completely consistent with the reported data for the inverse linear relation between T_c and T_m for Y:123, Bi:2223 and TI:2223 superconducting systems [77]. Although the T_c values are, respectively, 92, 110 and 125 K for the systems, the T_m are decreased to 1283, 1140 and 1080 K. These suggest that to get higher T_c, a eutectic compound of lower melting point should be looked for.

On the other hand, the phase diagram for undoped and doped high T_c systems is described by the following parabolic formula [78]:

$$p = \left[\frac{\left(1 - T_c^x/T_c^m\right)}{82.6}\right]^{\frac{1}{2}} + 0.16 \quad (7)$$

T_c^x and T_c^m are the critical and maximum critical temperatures, respectively; p is the hole-carrier concentration per Cu cation. Therefore, p, is established from the values of T_c and T_c^m listed in Table 4. It is clear that, p, is increased from 0.16 for pure sample to 0.20, 0.23 and 0.24 for La containing samples. However, this behavior occurs as a result of more positive charges transferred to the CuO_2 planes. This of course disagrees with the general role of substitution due to replacing Ca^{2+} by La^{+3}, and therefore, p, should be expected to decrease. However, according to the mechanism of excess oxygen in BSCCO system, the electrons are transferred from Cu to BiO layer leading to the formation of holes on Cu and electrons on Bi as follows; $Bi^{3+} + Cu^{2+} \rightarrow Bi^{3-x} + Cu^{2+x}$ [79]. These changes in the valence state of Bi are owing to excess oxygen and is reflected as the change of hole carriers of the system. To clarify this point according to the role of substitution, we supposed that La decreases the hole carrier concentration, and at the same time the excess oxygen introduces some excess holes in the Cu–O_2 planes, and consequently the effective (net) number of holes will be increased. This can be supported also by decreasing the doping distance and increasing the density of excess doping and excess oxygen as discussed in the above section.

3.4 Microhardness measurements

The apparent Vickers microhardness H_v is calculated by the following relation [80]:

$$H_v = 1854.4\left(\frac{F}{d_p^2}\right) \quad (8)$$

where H_v is given by GPa, d_p is the diagonal length of the indentation in μm and F is the applied load in N (F = 0.49, 0.981, 1.962, 2.942 and 4.904 N). It is obvious from H_v versus F curves shown in Fig. 5 that H_v decreases as the F increases up to 4.904 N. This behavior is nonlinear and usually due to increase in the mechanical penetration depth where the inner layers effect becomes more prominent as well as the well-known indentation size effect [80, 81].

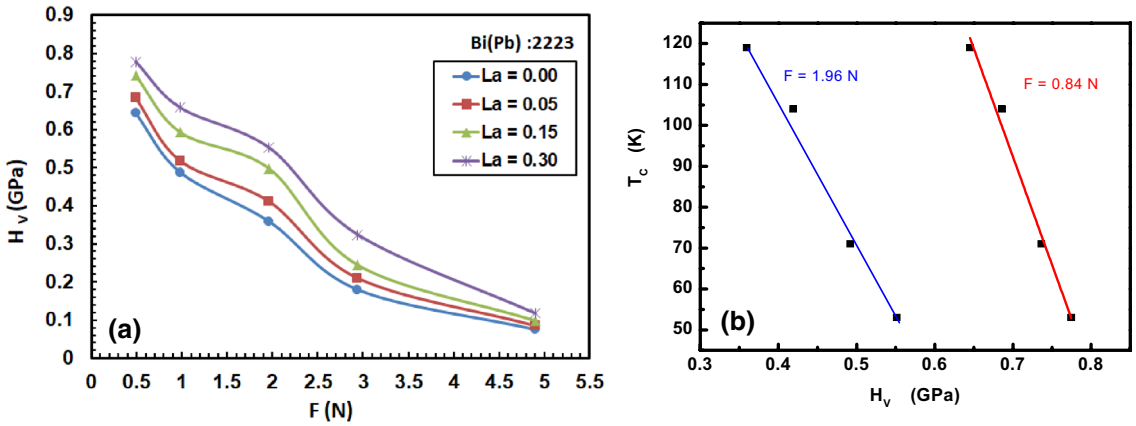

Fig. 5 **a** Measured Vickers hardness, H_V, against applied load, F, for the samples. **b** The correlation between the Vickers hardness, H_V, and the SC critical temperature, T_C, at two different applied loads as shown

Interestingly, at fixed F, the H_v is increased as La content increases [H_v α $(1/T_c)$] shown in Fig. 5b. Anyhow, the behavior of H_v against rare earth element RE^{3+} is normally controlled by the formation of impurity non-superconducting phases and irregularities. These phases and irregularities are mainly distributed at the grain boundaries, causes distortion of the bonding strength, and consequently the H_v decreases [45]. However, as indicated in the XRD analysis, we could not report these phases and also no significant change in the structure distortion *c/a* listed in Table 1 is nearly the same for all samples. Therefore, the increase of H_v values by La is probably due to the intercalation of La between superconducting grains in compositions which may be provide a plastic-flow region that allows relaxation of undesirable stresses resulting from the grain anisotropy of superconductors. This behavior is consistent with the reported elsewhere and indicated that H_v could be achieved by replacement of Ca by Y and Cd in BSCCO superconducting systems [40, 49, 51].

To test the original suggestion made by Matthias [1] for cooperative phenomenon. which link a normal state property to a superconducting property. Following Mathias [1] argument the relation between Vickers hardness and SC critical temperature, T_C, is tested as shown in Fig. 5b at two different applied loads. The obtained relation is a negatively sloped liner curves. This result indicates that both properties are strongly correlated and demonstrate a cooperative phenomenon as suggested earlier [1]. The linearity is tested and the following relations were produced to describe this phenomenon;

$$T_C = 249.64 - 357.6\,H_V \quad F = 1.96\ \text{N}$$
$$T_C = 462.17 - 528.4\,H_V \quad F = 0.84\ \text{N}$$

In addition, the elastic Young's modulus, E, and yield strength, Y, on the other hand are related to the H_v as follows [81, 82]

$$E = 81.9653H_v; \quad Y = \left(\frac{H_v}{3}\right) \tag{9}$$

However, a similar behavior of both, E, and, Y, against, F, and La content is obtained and shown in Fig. 6a and b as well as H_v behavior. This is probably due improving the roughness and interlayer bonding between grains when Ca is replaced by La.

Otherwise, the diagonal length d_p is strongly dependent on the applied load F according to [58, 83–85]:

$$\frac{F}{d_p} = H_t d_p + \gamma \tag{10}$$

where H_t is the true hardness and γ is the surface energy. The plots of (F/d_p) against d_p for lower and higher loads are shown in Fig. 7a and b, in which the slope represents H_t and the intercept represents γ. It is noted that the slope of the linear plot is positive for all samples at lower loads (0–1.962 N), while it is changed to negative at higher loads (2.94–4.90 N). The different values of H_t and γ are listed in Table 4. It is clear that H_t has a similar behavior of H_v against La concentration which indicating a decrease of crack faces and supporting hardness improvements. But the values of γ are decreased at lower loads from 0.01 N/μm for pure sample to 0.009, 0.008, 0.007 (N/μm) for La substituted samples, and from 0.019 N/μm to 0.021, 0.023, 0.027 N/μm at higher loads. From atomistic point of view, the more compacted surface the higher hardness and thus having lower surface energy as obtained. This is right for lower loads, but it is unclear at higher loads at present.

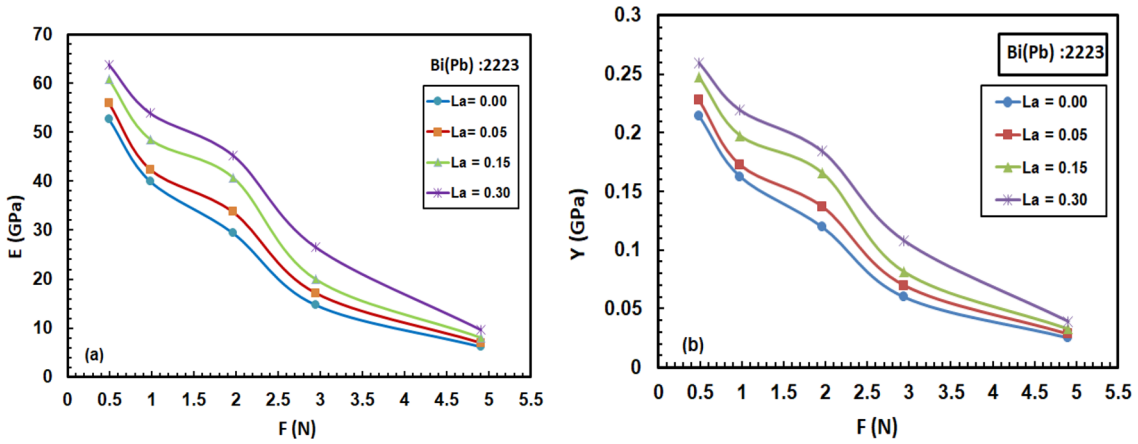

Fig. 6 **a**, **b** Young's modulus, E, and yield strength, Y, against applied load for the samples

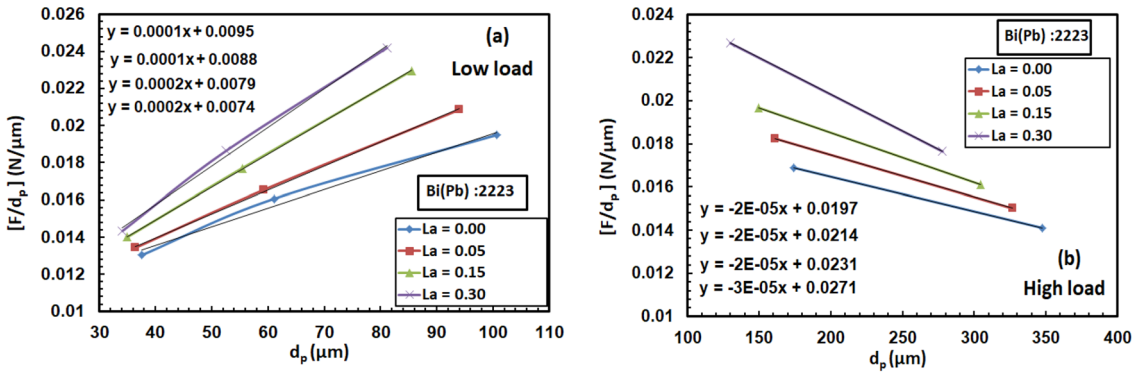

Fig. 7 **a**, **b** The plot of (F/d_p) against d_p at lower load for the samples

The indentation size effect observed in the present case can be explained by two different methods [86, 87]. The first method assumes that the indentation contains an elastic portion of the deformation which is supposed to relax upon loading beside plastic deformation. This can be accounted by adding an elastic component d_e to the measured in elastic d_p, supposing they are in the same direction, as follows [37, 88, 89];

$$H_t = 1854.4\left[\frac{F}{\left(d_p + d_e\right)^2}\right]$$
$$d_p = \left[(1854.4)^{\frac{1}{2}} H_t^{\frac{-1}{2}}\right] F^{\frac{1}{2}} - d_e \tag{11}$$

The plot of d_p versus $F^{1/2}$ is shown in Fig. 8a and b, in which the slope may be represented by $[(1854.4)^{1/2}(H_t)^{-1/2}]$, and the vertical intercept represents the d_e. It is clear that d_e values listed in Table 5 are decreased as La content increased, but their values at higher loads are more than that of lower loads. This of course emphasizes the hardness suppression as discussed above. It is decreased at lower loads from 26.76 μm for pure sample to 21.57, 15.73, 13.28 μm for La substituted samples, and from 421.66 to 406.91, 382.64, 379.55 μm at higher loads.

The second method considers energy dissipative processes and H_t can be defined by subtracting a dissipative part F_0 from the applied load F as follows [90, 91]:

$$H_t = 1854.4\left(\frac{F - F_o}{d_p^2}\right)$$
$$F = \left(\frac{H_t}{1854.4}\right) d_p^2 + F_o \tag{12}$$

The slope of linear plot of F against $d_p{}^2$ shown in Fig. 9 (a, b) represented by $(H_t/1854.4)$ while the intercept represents the resistance pressure F_o. It is clear that F_o values listed in Table 5 are slightly increased by La concentration, but their values at higher loads are more than that of lower loads. It is increased at lower loads from 0.201 N for pure

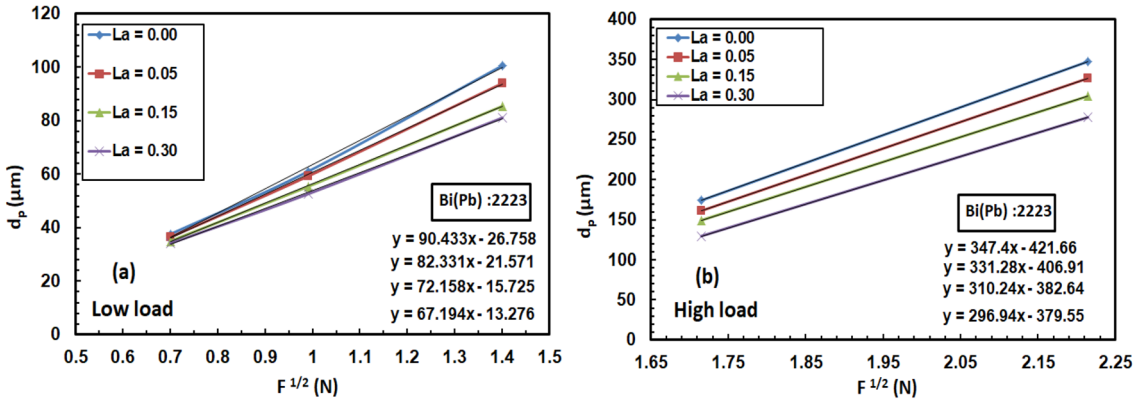

Fig. 8 **a**, **b** Measured indentation against lower and higher loads for the samples

Table 5 The H_t, γ, d_e and F_o for samples

La cont	H_t (GPa)	γ (N m)	d_e (μm)	F_o (N)
Low loads				
0.00	0.185	0.010	26.76	0.201
0.0	0.185	0.009	21.57	0.302
0.15	0.371	0.008	15.73	0.261
0.30	0.371	0.007	13.28	0.216
High loads				
0.0	− 0.037	0.019	421.66	2.28
0.05	− 0.037	0.021	406.91	2.31
0.15	− 0.037	0.023	382.64	2.32
0.30	0.056	0.027	379.55	2.39

sample to 0.302, 0.261 and 0.216 N for La containing samples, and from 2.28 to 2.31, 2.32, 2.39 N at higher loads.

Summing up the following points as obtained for the La substitution in place of Ca in the Bi (Pb):2223 ceramic superconducting system: (i) A clear 2223 majority single phase. (ii) increasing the carriers per Cu ion, effective Cu valence, critical concentration for quenching superconductivity, hardness and resistance pressure. (iii) decreasing the doping distance, crystal geometry factor, critical temperature, surface energy and elastic indentation. (vi) shifting endothermic peaks towered higher temperatures; (v) a sharp mass loss starting at about 800 °C.

There are several possible reasons for T_c suppression by La substituted at Ca site in Bi (Pb):2223 system as obtained in the present work. The first indicating that T_c depression is not related to the phase purity or bad microstructure in the form of secondary phases rich in Sr [92, 93]. The second reason indicated that the excess oxygen causing a tighter binding in the CuO_2 planes, and therefore, c-parameter orthorhombic distortion, excess oxygen, distance between Cu-atoms, density of excess doping, hole is reduced [60]. The third indicates that although La decreased the hole carriers, the excess oxygen is more than enough to compensate the variation of charge in the system, and consequently the number of holes in the CuO_2 planes increases. The fourth reason that may be put forward, as due to the verified correlations between the

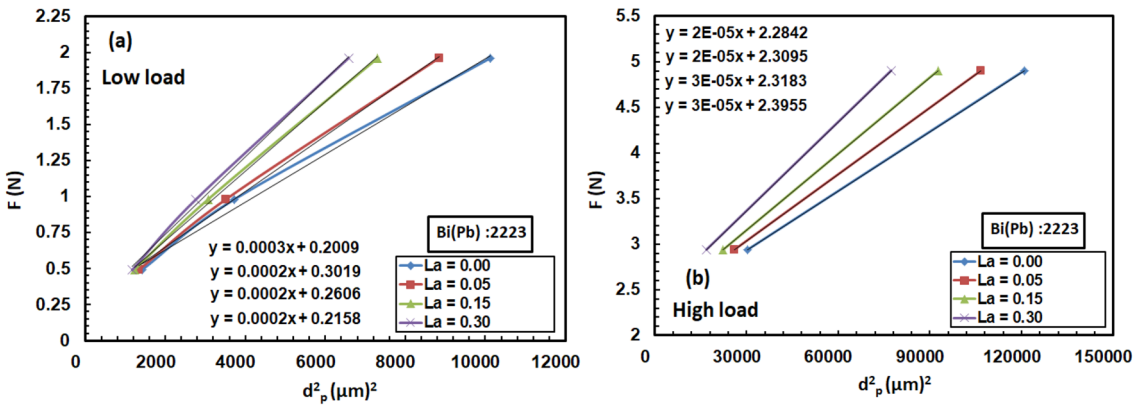

Fig. 9 **a**, **b** Applied load against measure elastic indentation for the samples. The straight curves are intended as a guide to the eye

melting temperature, hardness and SC critical temperature. These properties all have an origin related to some sort of electron–phonon interaction as all phenomenon are related to such a physical source; i.e. it may be said that there are an extended forces acting along such a wide temperature range.

Finally, the consistency of these points gives a fair degree of certainty to the suggestion of La substitution in place of Ca in Bi (Pb):2223 system.

4 Conclusion

Structural and different properties of $Bi_{1.7}Pb_{0.30}Sr_2Ca_{1-x}La_xCu_2O_y$ superconductor with various x values are investigated. We have shown that the replacement of Ca^{2+} by La^{3+} increased the excess oxygen, effective Cu valance and hole carrier per Cu ion. Further, the doping distance and crystal geometry factor are decreased, while the distance between Cu-atoms and density of excess doping are increased. Furthermore, a strong shift of endothermic peaks to higher temperatures and a sharp mass loss are obtained. Although the critical temperatures T_c are decreased by La, the critical concentration for quenching superconductivity may be extended above 0.30. Moreover, an inverse linear relation between T_m and T_c given by; $T_c\,(K) = 2200 - 2.462\,T_m$ could be obtained. On the other hand, Vickers hardness H_v is decreased by the applied loads F, but it is increased by increasing La content, i.e. $H_v \propto 1/T_c$. Although the variation of surface energy against La is found to be load dependent, the elastic indentation d_e are decreased and the resistance against pressure F_o is increased. But the values of F_o and d_e at higher loads are generally more than that of lower loads, while the vice is versa for the Y. The balance between the hole carriers lost by La^{3+} with that introduced by excess oxygen resulting for increasing the effective (net) of hole carriers. This of course helps for altering the quenching of superconductivity by La^{3+}, which highlights the present work.

References

1. B.T. Matthias, The Empirical Approach to Superconductivity, Chapter 7, in *Applied Solid State Physics*, ed. by W. Low, M. Schieber (Plenum Press, New York, 1970)
2. H. Maeda, Y. Tanaka, M. Fukutomi, T. Asano, Jpn. J. Appl. Phys. **27**(2), L209 (1988)
3. H.P. Roesera, F. Hetfleischa, F.M. Huberb, M.F. Von Schoenermarka, M. Steppera, A. Moritza, A.S. Nikoghosyanc, Acta Astronaut. **63**, 1372 (2008)
4. H. Eisaki, N. Kaneko, D.L. Feng, A. Damascelli, P.K. Mang, K.M. Shen, Z.X. Shen, M. Greven, Phys. Rev. B **69**, 064512 (2004)
5. P. Bordet, J.J. Capponi, C. Chaillout, J. Chenavas, A.W. Hewat, E.A. Hewat, J.L. Hodeau, M. Marezio, A. Narliker (Ed.), vol. 2, Nova Science Publisher, p. 171 (1991).
6. A. Amirabadizadeh, S. Memarzadeh, N. Tajabor, H. Arabi, World J. Condens. Matter Phys. **2**, 148 (2012)
7. I.H. Gul, M.A. Rehman, M. Ali, A. Maqsood, Physica C **432**(1–2), 71 (2005)
8. A. Ehmann et al., J. Less Common Met. **151**, 55 (1959)
9. A. Jeremie, K.A. Yadri, J.C. Grivel, R. Fiñkiger, Supercond. Sci. Technol. **6**, 730 (1993)
10. M.A. Aksan, M.E. Yakinci, J. Alloy Compd. **433**, 22 (2007)
11. C.H. Hwang, G. Kim, Supercond. Sci. Technol. **5**, 586 (1992)
12. H.A. Qureshi, M. Arshad, K.S. Durrani, Waqas H **94**, 175 (2008)
13. S.B.M. Dogruer, G.Y.A. Varilci, C.T.Y. Zalaoglu, J. Supercond. Novel Magn. **25**, 847 (2012)
14. A.V. Pop, G. Ilonca, D. Ciurchea, V. Pop, I.G. Deac, Phys. B **284–288**, 1101 (2000)
15. M.A.M.C. Kaya, B. Ozcelik, B. Ozkurt, A. Sotelo, J. Mater. Sci. Mater. Electron. **24**, 1580 (2013)
16. S. Vinu, P.M. Sarun, A. Biju, R. Shabna, P. Guruswamy, Supercond. Sci. Technol. **21**, 3 (2008)
17. M.A.S. Aksan, Y. Balci, M.E. Yakinci, Mater. Chem. Phys. **106**, 428 (2007)
18. C.A.M. dos Santos, S. Moehlecke, Y. Kopelevich, A.J.S. Machado, Physica C **390**, 21 (2003)
19. A.Y. Ilyushchkin, T. Yamashita, L. Boskovic, I.D.R. Mackinnon, Supercond. Sci. Technol. **17**, 1201 (2004)
20. A. Sedky, Physica C **468**, 1041 (2008)
21. S. Singh, Physica C **294**, 249 (1998)
22. K. Nanda Kishore, S. Satyavathi, M. Muralidhar, O. Pena, V. Hari Babu, Physica C **252**, 49 (1995)
23. A. Sedky, J. Phys. Chem. Solids **70**, 483 (2009)
24. A. Sedky, J. Alloys Compd. **499**, 238 (2010)
25. D. Marconi, G. Stiufiuc, A.V. Pop, J. Phys. Conf. Ser. **153**, 012022 (2009)
26. B. Chevalier et al., Mater. Sci. Eng. B **2**, 277 (1989)
27. M.A. Aksan, S. Altin, M.E. Yakinci, A. Guldeste, Y. Balci, J. Mater. Sci. Technol. **27**(1), 314 (2011)
28. S. Altin, M.A. Aksan, M.E. Yakinci, Mater. Chem. Phys. **133**(2–3), 706 (2012)
29. B. Jayaram, P.C. Lanchester, M.T. Weller, Physica C **160**, 17 (1989)
30. A. Coskun, A. Ekicibil, B. Ozcelik, K. Kiymac, Chin. Phys. Lett. **21**, 2041 (2004)
31. P. SumanaPrabhu, M.S. RamachandraRao, U.V. Varadaraju, G.V. SubbaRao, Phys. Rev. B **50**, 6929 (1994)
32. V.P.S. Awana, S.K. Agarwal, R. Ray, S. Gupta, A.V. Narlikar, Physica C **43**, 191 (1992)
33. J.M. Tarason, P. Barboux, G.W. Hull, R. Ramesh, L.H. Greene, M. Giroud, M.S. Hegde, W.R. Mckinnon, Phys. Rev. B **39**, 4316 (1989)
34. K. Koyama, S. Kanno, S. Noguchi, Jpn. J. Appl. Phys. **29**, L53 (1990)
35. H. Jin, J. Kotzler, Physica C **325**, 153 (1999)
36. N. Hudakova, Physica C **406**, 58 (2004)
37. A.D.M. dos Santos, G.S. Pinto, B. Ferreira, A.J.S. Machado, Physica C **354**, 388 (2001)
38. S. Kobayashi, N. Suzuki, Physica C **185–189**, 869 (1991)
39. Q. Cao, K.Q. Ruan, S.Y. Li, X.H. Chen, G.G. Qian, L.Z. Cao, Physica C **334**, 237 (2000)
40. S.M. Khalil, J. Phys. Chem. Solids **64**, 855 (2003)
41. X. Sun, X. Zhao, W. Wu, X. Fan, X.-G. Li, H.C. Ku, Physica C **307**, 7 (1998)
42. X. Zhao, X. Sun, X. Fan, W. Wu, X.G. Li, S. Guo, Z. Zhao, Physica C **307**, 265 (1998)

43. M. Yilmazlar, H.A. Cetinkara, M. Nursoy, O. Ozturk, C. Terzioglu, Physica C **442**, 101 (2006)
44. K.A. Jassim, T.J. Alwan, J. Supercond. Nov. Magn. **22**, 861 (2009)
45. H. Aydin, O. Cakiroglu, M. Nursoy, C. Terzioglu, Chin. J. Phys. **47**(2), 192 (2009)
46. S.M. Khalil, J. Phys. Chem. Solids **62**(3), 457 (2001)
47. A.A. Elmustafa, D.S. Stone, J. Mech. Phys. Solid **51**, 357 (2003)
48. K. Sangwal, Mater. Chem. Phys. **63**, 145 (2000)
49. M.M. Abbas, Int. J. Curr. Eng. Technol. **5**(3), 1908 (2015)
50. S.M. Khalil, Smart Mater. Struct. **14**, 804 (2005)
51. S.M. Khalil, J. Low. Temp. Phys. **143**(112), 31 (2006)
52. I.K. Schuller, J.D. Jorgfnsen, MRS Bull. **14**, 27 (1989)
53. S.M. Khalil, A. Sedky, Phys. B **357**, 299 (2005)
54. A. Simon, P.S. Mukherjee, M.S. Sarma, A.D. Damodaran, J. Mater. Sci. **29**, 5059 (1994)
55. S.A. Halim, S.B. Mohamed, H. Azhan, S.A. Khawaldeh, H.A.A. Sidek, Physica C **312**, 78 (1999)
56. M.S. Lee, K.Y. Song, Supercond. Sci. Technol. **15**, 851 (2002)
57. A.I. Malik, S. Celebi, S.A. Halim, Physica C **377**, 421 (2002)
58. J. Gong, J. Wu, Z. Guan, J. Eur. Ceram. Soc. **19**(15), 2625 (1999)
59. R. Singth, A. Gupta, S.K. Agarwal, D.P. Singh, A.V. Narlikar, Supercond. Sci. Technol. **10**, 1 (1997)
60. F. Munakata, T. Kawano, H. Yamauchi, Y. Inoue, Physica C **190**, 471 (1992)
61. S. Sedky, A. Gupta, V.P.S. Awana, A.V. Narlikar, Phys. Rev. B **58**(18), 12495 (1998)
62. P. Mandel, A. Poddar, B. Ghosh, P. Choudhury, Phys. Rev. B **43**(16), 13102 (1991)
63. A. Biju, P.M. Sarun, R.P. Aloysius, Physica C **433**, 68 (2007)
64. W.M. Chen, X.S. Wu, J.F. Geng, J. Chen, D.B. Chen, X. Jin, S.S. Jiang, J. Superconduct **10**(1), 41 (1997)
65. J. Hwang, T. Timusk, G.D. Gu, Nature **427**, 714 (2004)
66. F. Jean, G. Collin, M. Andrieux, N. Blanchard, J.F. Marucco, Physics C **339**, 269 (2000)
67. M.R. Norman, H. Ding, M. Randeria, J.C. Campuzano, T. Yokoya, T. Takeuchi, T. Takahashi, T. Mochiku, K. Kadowaki, P. Guptasarma, D.H. Hinks, Nature **392**, 157 (1998)
68. J.W. Alldredge, J. Lee, K. McElroy, M. Wang, K. Fujita, Y. Kohsaka, C. Taylor, H. Eisaki, S. Uchida, P.J. Hirschfeld, J.C. Davis, Nat. Phys. **4**, 319 (2008)
69. H.P. Roesera, F.M. Huberb, M.F. von Schoenermarka, A.S. Nikoghosyanc, Acta Astronaut. **65**, 489–494 (2009)
70. S. Bernik, M. Hrovat, D. Kolar, Supercond. Sci. Technol. **7**, 920 (1994)
71. T. Honda, T. Wada, M. Sakai, M. Miyanaga, N. Nishikawa, S. Uchida, K. Uchinokawa, S. Tanaka, Jpn. J. Appl. Phys. **27**, L545 (1988)
72. A. Broido, J. Polym. Sci. A **7**, 1761 (1969)
73. R. Venkataramani, S.P. Garg, S. Mazumder, Bull. Mater. Sci. **14**(3), 665 (1991)
74. S. Ravi, V. SeshuBai, Phys. Rev. B **49**, 13082 (1994)
75. R.K. Nkum, W.R. Datars, Supercond. Sci. Technol. **8**, 822 (1995)
76. M.R. Presland, J.L. Tallon, R.G. Buckley, R.S. Liu, N.E. Floer, Physica C **176**, 95 (1991)
77. A.A. Bahgat, High TC Updata (USA) Technical Report **6**(19), 5 (1992). https://doi.org/10.13140/RG.2.2.13407.25761
78. P. Konsin, B. Sorkin, Supercond. Sci. Technol. **13**, 301 (2000)
79. A. Leenders, M. Ullrich, H.C. Freyhardt, Physica C **279**, 173 (1997)
80. C. Veerender, V.R. Dumke, M. Nagabhooshanam, Phys. Status Solid A **144**, 199 (1994)
81. D. Tabor, *The Hardness of Metals* (Clarendon, Oxford, 1951)
82. B.R. Lawn, T.R. Wilshaw, J. Mater. Sci. **10**, 1049 (1975)
83. H.A. Cetinkara, M. Nursoy, O. Ozturk, C. Terzioglu, Physica C **442**, 101 (2006)
84. J.B. Quinn, G.D. Quinn, J. Mater. Sci. **32**, 4331 (1997)
85. A.K. Dutta, N. Narasaiah, A.B. Chattopadhyaya, K.K. Ray, Ceram. Int. **27**, 407 (2001)
86. B.Y. Farber et al., Superconductivity **4**, 2296 (1991)
87. F. Frohlinch, P. Grau, W. Grellmann, Phys. Status Solidi **42**, 79 (1997)
88. H. Li, R.C. Bradt, J. Mater. Sci. **22**, 917 (1993)
89. C. Hays, E.G. Kendall, Metallography **6**(4), 275 (1973)
90. J. Gong, J. Wu, Z. Guan, J. Eur. Ceram. Soc. **19**, 2625 (1999)
91. Z. Li, A. Ghosh, A.S. Kobayashi, J. Ami Soc. **72**, 904 (1989)
92. V.G. Prabitha, A. Biju, R.G. Abhilash Kumar, P.M. Sarun, R.P. Aloysius, U. Syamaprasad, Physica C **433**, 28 (2005)
93. A. Biju, R.P. Aloysius, U. Syamaprasad, Physica C **440**, 52 (2006)